JOURNAL OF PROPULSION AND POWER
Vol. 11, No. 1, January–February 1995

Deficiencies and Requirements in Modeling of Slag Generation in Solid Rocket Motors

Mark Salita*
Analytical Methods, Inc., Ogden, Utah 84403

The slag generation process is very complex and involves unsteady viscous two-phase flow with recirculating dense-droplet swirling clouds, multimodal droplet size distributions, and droplet/wall interactions in motors that may be vectoring, spinning, accelerating axially, and ejecting slag. Recently-published models of slag accumulation have oversimplified this phenomenon to the extent that the accuracy of their predictions is questionable and the conclusions drawn from their modeling may be misleading. The purpose of this article is to summarize what is known and what is not known about slag generation, to expose current modeling deficiencies, and to identify the minimum requirements for future slag modeling. In particular, clues from a large body of static motor data are summarized, the inadequacies of potential-flow modeling are discussed, misconceptions of droplet size distributions and bulk density are corrected, and the importance of capture rules and propellant variability are described.

Nomenclature

C_D = droplet drag coefficient
D = droplet diameter
F = mass fraction of products as Al_2O_3
$f(D)$ = mass fraction of droplets with diameters less than D
g = acceleration
m = mass flow rate
Re = Reynolds number
r = propellant burn rate
T = temperature
u, v = normalized velocity components in x and y directions
w = generalized velocity component
x, y = normalized axial and radial directions in motor chamber
β = droplet combustion fraction D_m/D_{ag}
μ = gas viscosity
ρ = mass density
σ = standard deviation of droplet size distribution
τ = normalized time
ϕ = mass fraction of aluminum in propellant
Ψ = local value of stream function
ω = local vorticity of gas flowfield

Subscripts
ag = aluminum agglomerate
d = droplet
g = gas
m = mass median
n = index of discrete droplet size
p = propellant

Introduction

MANY solid rockets use aluminized propellants and submerged nozzles to improve performance. When these propellants burn, the aluminum powder melts to form agglomerates on the propellant surface. These agglomerates either stream along the surface and onto the case wall, or are ejected into the highly rotational flow where they burn almost completely to a bimodal log-normal size-distribution of liquid aluminum oxide (Al_2O_3) droplets.[1,2] Slag is generated when the wall streaming or gas-field driven droplets become trapped behind the submerged nozzle (Fig. 1). This entrapment occurs either by impingement on some portion of the backface of the nozzle, or by capture in a recirculation zone that has been observed experimentally in water table tests[3] (Fig. 2), water-tunnel tests,[4] cold-flow tests,[5] and real time x-ray radiography (RTR) of burning full-scale boosters. Evidence of wall streaming and impingement-layer formation is suggested by the schematic of the Titan IV SRMU slag discovered at the end of motor burn (Fig. 3). The tendency for entrapment increases with droplet diameter, bulk density, velocity, and radial distance of the trajectory from the motor centerline. Chemical analysis of the slag generally shows it to contain less than 2% unburned aluminum, but larger amounts of unburned aluminum may have existed before CO_2 or water quench provided postburn oxidizing potential. Slag reduces motor performance and has been postulated to cause 1) both excessive and reduced erosion of aft-dome insulation, 2) ejection-induced thrust and sideforce, and 3) vehicle nutation ("coning") due to sloshing in spinning motors.

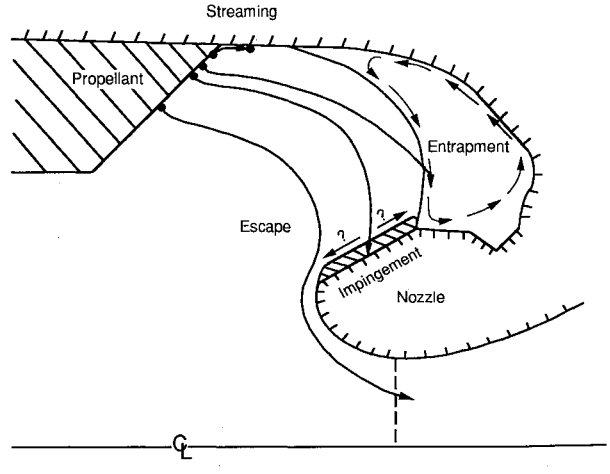

Fig. 1 Scenarios of slag accumulation: wall streaming and two-phase flow with entrapment and impingement that may be retained.

Received July 1, 1993; revision received May 1, 1994; accepted for publication May 18, 1994. Copyright © 1994 by M. Salita. Published by the American Institute of Aeronautics and Astronautics, Inc., with permission.

*Thiokol Corporation; currently Senior Scientist, TRW Ballistic Missile Division.

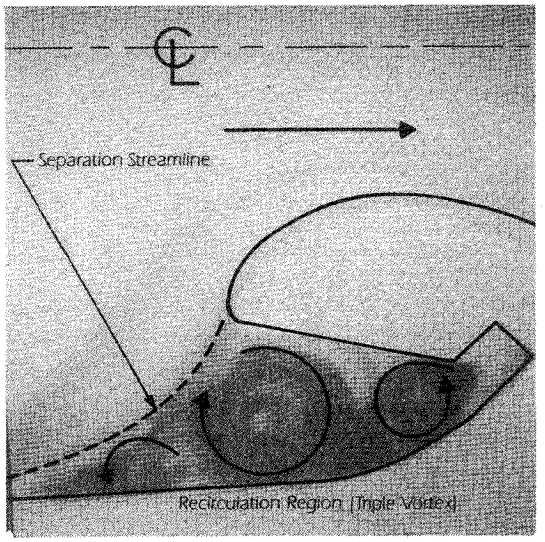

Fig. 2 Experimental evidence of recirculation zone behind submerged nozzle in water table simulation of RSRM aftend.

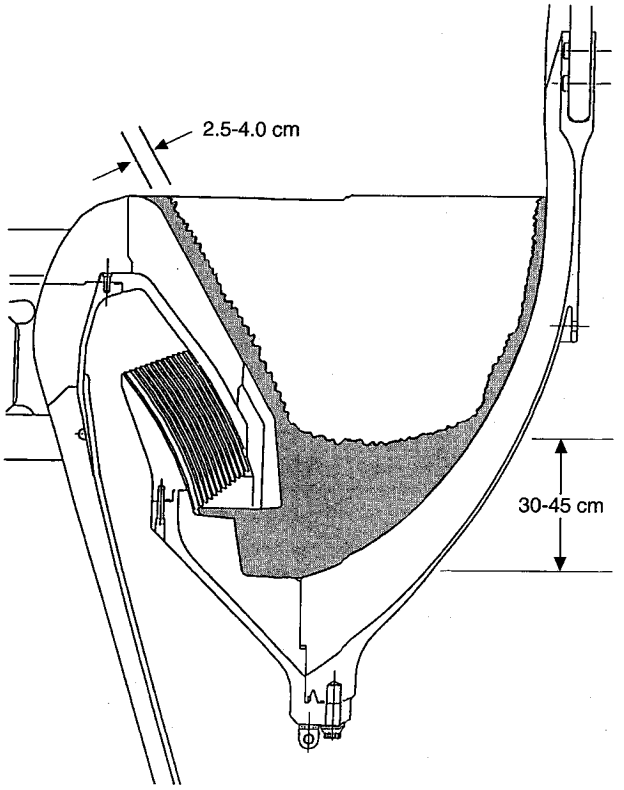

Fig. 3 Evidence of slag layers along case wall and nozzle backface: postfire slag deposition in SRMU.

Surprising magnitude and/or variability of slag weight has occurred in many motors, which has prompted numerous attempts to model the phenomenon. This modeling requires four steps: 1) prediction of the gas flowfield, 2) knowledge of the size distribution and bulk density of the Al_2O_3 droplets, 3) prediction of the droplet trajectories, and 4) identification of the "capture rules," defining which droplets will be retained in the motor as slag. Unfortunately, recent publications in the open literature[6-11] have oversimplified the flowfield modeling as irrotational and inviscid, ignored the uncertainty of the capture rules, and/or chosen erroneous droplet data so that their predictions may be meaningless and misleading.

Even when models are applied that use measured droplet size data and gasdynamics that is either rotational inviscid[12] or rotational viscous,[13-15] the identification of correct capture rules is uncertain, and key mechanisms of slag accumulation may be overlooked. Indeed, recent RTR movies of burning full-scale boosters suggest a flow complexity that may be beyond the simulation ability of even modern viscous flow models using measured droplet sizes.

The purpose of this article is 1) to summarize what is known and not known about slag generation, 2) to expose the deficiencies of slag-generation models that have recently been published in the open literature, and 3) to propose a more rigorous methodology for modeling slag generation.

Consequently, 1) the slag data for five motors of current interest is summarized, 2) the best available data for droplet size distribution and bulk density is presented, 3) the uncertainty of the capture rules for droplet entrapment is discussed, and 4) the inappropriate use of potential (irrotational, inviscid) flow models is demonstrated and improved models are described. Common modeling deficiencies are summarized, and a series of steps is proposed that is required to make improved predictions of slag weight.

Table 1 Measured slag weights for statically fired Space Shuttle Boosters

Version	Motor	Weight, kg (lbm)	Comments
STD	DM-1	290 (639)	
	DM-2	300 (659)	
	DM-3	198 (435)	KM, PE/lot 5
	DM-4	301 (663)	
	QM-1	225 (496)	
	QM-2	970 (2134)	KM/lot 25, 74°F
	QM-3	362 (797)	KM/lot 9, 73°F
	Average	378 (832)	0.26% of Al_2O_3, max/min = 4.9
HPM	DM-5	211 (465)	New, 72°F, PE/lot 32
	QM-4	475 (1046)	New, 76°F, PE/lot 33
	ETM-1	1535 (3377)	Old, 71°F, KM/lot 59
	TEM-1	719 (1582)	Old, 71°F, unvectored
	TEM-2	1207 (2656)	Old, 67°F, unvectored
	TEM-3	1316 (2895)	Old, 70°F, unvectored
	TEM-4	426 (937)	Old, 80°F, unvectored
	TEM-5	998 (2195)	Old, 72°F, unvecxtored
	TEM-6	1407 (3095)	Old, 69°F, unvectored
	TEM-7	824 (1813)	Old, 68°F, vectored
	TEM-8	825 (1815)	Old, 80°F, vectored
	TEM-9	955 (2100)	Old, 73°F, unvectored
	TEM-10	1021 (2246)	Old, 70°F, unvectored, RTR
	TEM-11	1300 (2860)	Old, 79°F, RTR, 5.5° pitch at 67,90 s
	Average	944 (2077)	0.66% of Al_2O_3, max/min = 7.2
RSRM	DM-8	1082 (2381)	PE/lot 69, 76°F, QPCB
	DM-9	1032 (2270)	PE/lot 69, 64°F, QPCB
	QM-6	616 (1355)	KM, 70°F
	QM-7	916 (2016)	KM, 92°F
	QM-8	1000 (2201)	PE, 39°F
	PVM-1	680 (1497)	PE, 79°F
	Average	888 (1953)	0.62% of Al_2O_3, max/min = 1.8
	FSM-1	212 (466)	All WECCO/lot 109, 82°F
	FSM-2	1096 (2411)	All WECCO except aft-center = KM, 69°F
	FSM-3	257 (565)	All WECCO/2 lots except forward = KM, 78°F
	FSM-4	598 (1315)	All WECCO
	Average	541 (1190)	Aft-center segment big slag contributor
FWC	DM-6	157 (346)	PE/lot 62, 74°F
	DM-7	180 (396)	PE/lot 63, 75°F
	Average	169 (371)	0.12% of Al_2O_3, max/min = 1.1

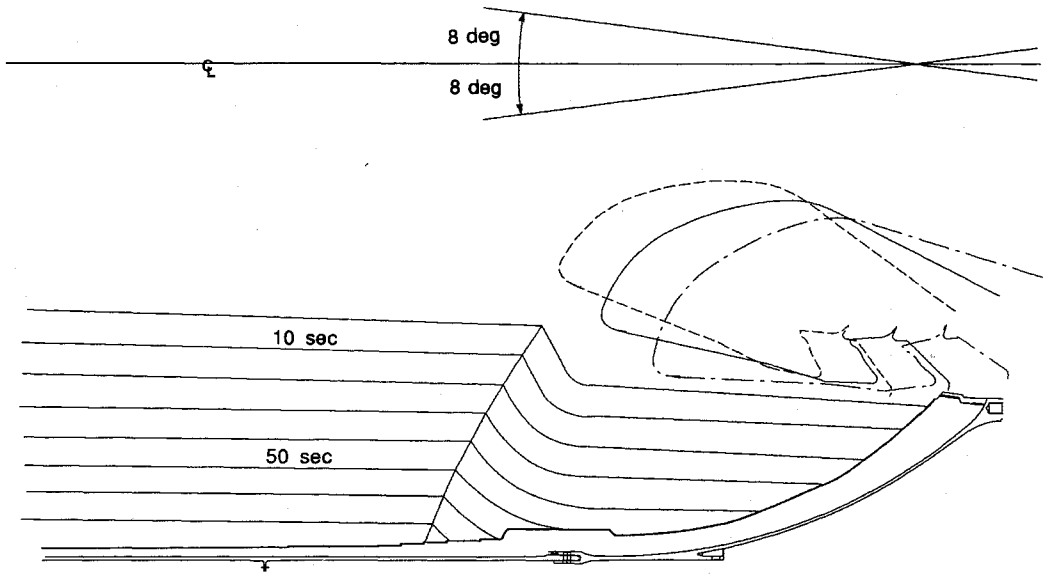

Fig. 4 RSRM aftend showing brain burnback pattern and nozzle vectoring limits.

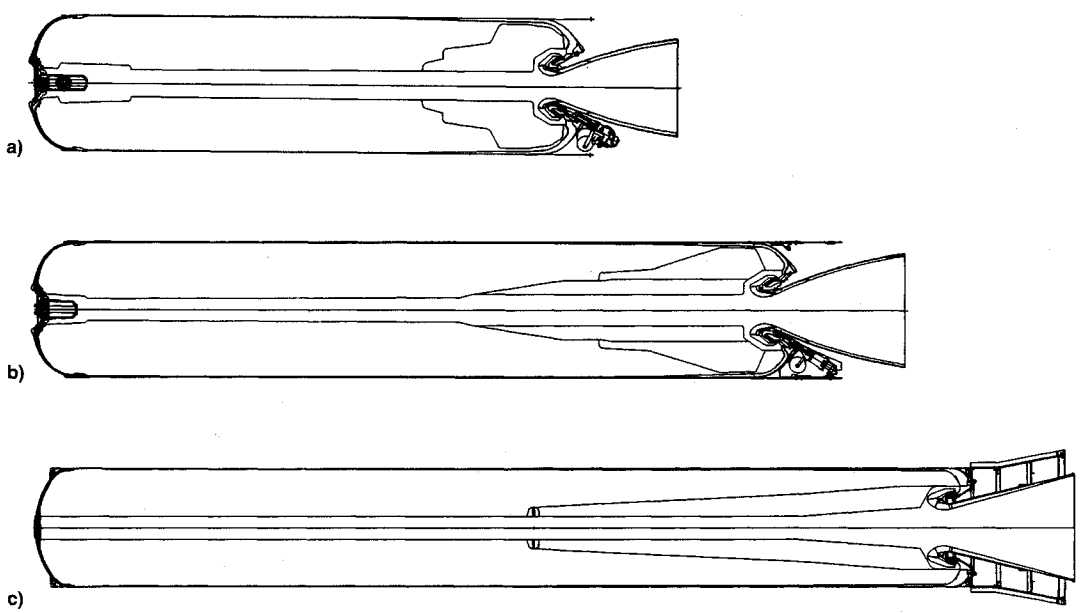

Fig. 5 Solid boosters with long tapered aft-fins: a) SICBM short motor, b) SICBM long motor, and c) Castor IVB.

Motor Slag Weights

Slag weights measured after the static firings of four different booster motors including the Space Shuttle Booster (Fig. 4), SICBM short and long motors (Fig. 5), Castor IVB (Fig. 5), and Titan IV SRMU (Fig. 6) are summarized in Tables 1–4, and the slag-related properties of their propellants are summarized in Table 5. It is important to recognize that the actual slag weights accumulated at least temporarily during motor burn may be larger due to ejection of some of the slag. Insulation erosion patterns have generally not been used to identify slag accumulation mechanisms and location because of the difficulty of isolating the multiple effects of convective and radiative heating, cookoff, droplet impingement erosion, and slag-layer shielding. RTR videos of aft-end chamber flow are available for the redesigned Shuttle Booster (RSRM), SICBM, and SRMU; although the RSRM RTR has a limited field of view and resolution.

The biggest data base has been obtained from 33 horizontal static firings of the Space Shuttle Booster (Table 1), but encompasses four slightly different configurations [the original "standard" (STD) design, the higher-performance design

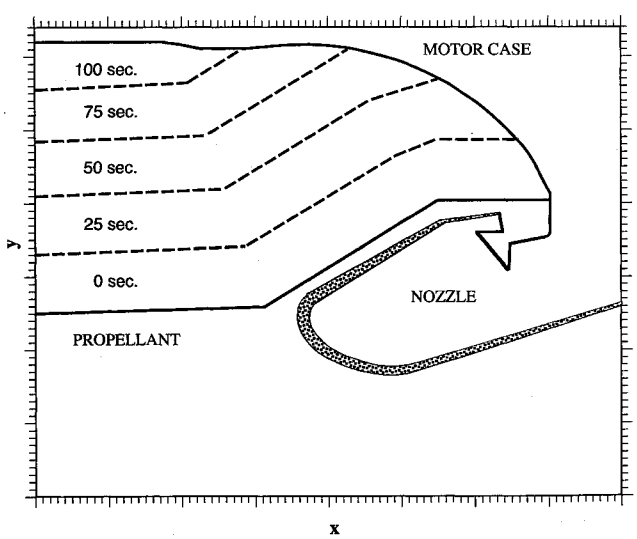

Fig. 6 Burnback pattern of aft segment of Titan IV (SRMU) booster.

(HPM), the RSRM, and the filament-wound-case motor (FWC)], as well as three different ammonium perchlorate (AP) vendors (PE = Pacific Engineering, KM = Kerr-McGee, WECCO = Western Electrochemical Company). The AP vendors and lots are shown in Table 1 only if a motor used only one. All motors conducted a relatively standard vector duty cycle unless noted. The following observations can be made:

1) Excluding QM-2, the STD motors averaged low slag weight [280 kg (615 lbm)] with low variation (±30%).

2) The HPM chamber configuration differed from STD mainly in the amount of inhibitor on the intersegment slots, yet averaged about two and a half times the slag weight with a variation over a factor of 7.

3) The six RSRM motors with KM or PE AP generated nearly the same average slag weight as the HPM motors, but with much less variation (±30%).

4) The 3 RSRM/FSM motors suggest that propellant with WECCO AP generates much less slag than that with KM or PE AP, since the forward KM segment in FSM-3 is not expected to contribute to slag, whereas the aft-center KM segment in FSM-2 will contribute significantly to slag.

5) Two motors (DM-8,9) with the same AP vendor and lot generated nearly identical slag weights.

6) The two FWC motors both generated the same low slag weight.

7) Motor age alone does not seem to be a factor since old TEM motors generated both low and high slag weights, whereas younger motors generated both low slag (HPM) and high slag (RSRM).

8) Nozzle vectoring has been proposed as a source of slag ejection, yet the motor with the highest slag (ETM-1) was vectored, whereas the HPM/RSRM with the second smallest (TEM-4) was not. A large (5.5 deg) nosedown pitch at 67 s in TEM-11 generated a 0.083-MPa (12-psi) pressure pulse that RTR and plume radiography suggested was due to slag ejection; a comparable pitch at 90 s yielded no pulse. Nozzle vectoring may induce enough slag ejection to affect vehicle control without affecting the total slag weight significantly.

9) Comparison of TEM-1,6 and QM-8/DM-9 shows that mean bulk temperature of the propellant does not seem to affect slag weight as it does in the SRMU (Table 4).

The data raises the following questions about Shuttle Booster slag:

1) Why did the QM-2 motor have two and a half times the slag weight of the other 6 STD motors?

2) Why did the slag weights in the HPM motors average so much higher and vary so much more than in the STD motors?

3) Why does WECCO AP appear to yield so much less slag than KM and PE?

The effect of subtle variability in propellant formulation has proven enigmatic: recent combustion bomb tests at Thiokol and the Naval Air Warfare Center[16] (NAWC) have shown no significant differences in size distribution of the aluminum oxide droplets among propellant samples using either WECCO or KM or PE AP, whereas Hutchison[49] has correlated RSRM slag weight variation with small variability in the size of the AP crystals in the propellant.

Slag data exists for two versions of the SICBM (Table 2), a short (30K) chamber and a lengthened (37K) chamber with an extended rear fin region. The following questions are raised:

1) Why did the short 30K motor have an average slag weight comparable to the Shuttle Booster, but the long-finned 37 K version had almost three times the slag percentage even though quench bomb measurements (Table 5) show that the mass-median diameter of the large droplets generated by the SICBM

Table 2 Measured slag weights for statically fired SICBM motors

Version	Motor	Weight, kg (lbm)	Comments
Short	DS-1	20 (43)	All fired horizontally
	DS-2	15 (33)	
	DS-3	25 (55)	
	Average	20 (44)	0.55% of Al_2O_3, max/min = 1.7
Long	DS-4	50 (110)	All except DM-8 fired horizontally
	DS-5	42 (93)	
	DS-6	61 (134)	RTR
	DS-7	64 (141)	RTR
	DS-8	53 (116)	Fired vertically with RTR
	FPT-1	69 (151)	
	FPT-2	64 (141)	
	FPT-3	63 (138)	
	Average	58 (128)	1.59% of Al_2O_3, max/min = 1.6

Table 3 Measured slag weights for statically fired Castor IVB boosters

Motor	Weight, kg (lbm)	Comments
1	4.1 (9)	All fired horizontally
2	5.0 (11)	
3	6.8 (15)	
Average	5.0 (11)	0.17% of Al_2O_3

Table 4 Measured slag weights for statically fired Titan IV SRMU boosters

Motor	Weight, kg (lbm)	Comments
PQM-1′	2015 (4434)	60°F, KM, RTR
QM-1	1897 (4174)	60°F, WECCO
QM-2	1847 (4064)	40°F, KM, RTR
QM-3	2137 (4701)	90°F, WECCO
QM-4	2021 (4447)	40°F, KM
Average	1985 (4366)	1.90% of Al_2O_3, max/min = 1.1

Table 5 Propellant data

Parameter	RSRM/HPM	Titan SRMU	SICBM/37K	Castor IVB	Star-48
Designation	TP-H1148	QDC	TP-N1040	TP-H8299	TP-H3340
Total weight, lbm	1,100,000	695,000	25,400	18,000	Variable
% Aluminum	16.0	19.0	18.0	20.0	18.0
% AP	69.0	69.0	9.0	69.0	71.0
% Al_2O_3 (100F)	28.8	33.5	31.7	34.7	31.9
p_{ref}, MPa	4.31	6.90	6.90	3.45	3.45
p_{ref}, psi	625	1,000	1,000	500	500
D_m, μm @ p_{ref}	115	120	55	131	130
Source of D_m	QPCB	Eq. (2)	QPCB	Eq. (2)	QPCB
Axial slots (fins)	Head-end	Head-end	Aft-end	Aft-end	Aft-end

propellant is less than half that generated by the Shuttle Booster propellant?

2) Why is the variation of ±25% in slag weight for each version much smaller than in the Shuttle Booster?

RTR of the only vertically fired motor (DS-8) has been analyzed digitally by Frederick[17] and reveals the following behavior of the growth of the slag pool (Fig. 7): 1) slag accumulation begins much earlier in the motor burn than originally believed, 2) the growth in slag pool volume is roughly linear until about 32 s (75% of motor action time), 3) between 32 s and tailoff the slag pool volume is nearly constant at a value whose mass of 116 lbm is identical to that measured after quench and cooldown (assuming the conventional choice of 100 lbm/ft^3 for hot slag density), and 4) at the end of tailoff boiling of the slag pool increases its volume, but only to about half the submergence volume so that significant slag ejection is unlikely (which is consistent with the equivalence of plateau and postfire slag mass). SICBM DS-8 is the only booster known to have been fired both vertically and horizontally, and the measured slag weights were roughly the same. The cause of the plateau in slag pool volume after 32 s has as yet only been speculated.

The Castor IVB is essentially the same as the Castor IVA except that the nozzle has been submerged. Three verification motors were fired horizontally, and the slag weights were surprisingly small and repeatable (Table 3). Understanding why so little slag was generated in this motor is the key to understanding the slag generation process in all motors and reducing slag by design.

Five Titan IV SRMU boosters have thus far been fired, all vertically; slag weights were surprisingly large and repeatable (Table 4). The slag weight is seen to increase with propellant mean bulk temperature. The history of slag "pool" growth (Fig. 8) has been deduced from enhanced RTR[12] of the vertically fired motor QM-2 and is surprisingly similar to that deduced from the SICBM RTR, specifically: 1) roughly linear growth between motor ignition and 100 s (72% of action time), 2) a plateau in pool depth between 100 s and tailoff whose mass corresponds nearly to the postfire measured slag weight, and 3) boiling at the end of tailoff to a pool volume only half that of the submergence volume. The cause of the plateau can as yet only be speculated, but slag ejection in QM-2 appears unlikely.

The variation of slag weight in statically fired STAR-48 space motors (Fig. 9) varies bilinearly with spin rate above a threshhold of about 25 rpm; Eber[18] has also been able to correlate this data with net droplet acceleration (above an axial threshhold) at the propellant surface. In addition, Marin[50] showed with spinning Bates motors that the particle size of aluminum in the propellant can have a significant effect on agglomeration and, therefore, on oxide droplet sizes.

Hence, the following questions must be asked about slag in statically fired motors:

1) Why do motors with the largest slag weight percentages (SICBM and Titan IV) have the smallest motor-to-motor variation in slag. Could it be that their submergence cavities are "full" of slag?

2) Why do motors with similar (%Al, AP) AP-composite propellants generate both the smallest (Castor IVB) and the largest (SRMU) slag weight fraction in the data base?

3) Why do the slag weights in the Shuttle Boosters vary by a factor of 7 in spite of its high level of quality control?

4) Why did slag triple in SICBM when the motor was lengthened by 35% by extending the fin region?

5) Why are the slag weights in SICBM so large even though the measured droplet sizes are half those of the Shuttle Booster?

6) Why are the slag weights in Castor IVB so low even though the propellant contains 20% aluminum and has a long tapered aft-end fin like SICBM which had high slag?

7) Why are the slag weights in SRMU so large and invariant even though its grain design and estimated droplet sizes are similar to those in the Shuttle Booster?

8) What criteria control slag retention and ejection and what would the slag weights be if none were ejected out the nozzle?

9) What causes the threshhold in slag accumulation in spinning space motors?

Only when these questions are answered will the mechanisms driving slag generation be understood well enough to design motors to minimize slag. In particular, it is desirable to identify the attribute of the Castor IVB design that resulted in low slag so that future motors can be designed to take advantage of that attribute. This would be far more effective than the proposal by Fendell et al.[8] to reduce the aluminum fraction in that region of propellant from which slag originates.

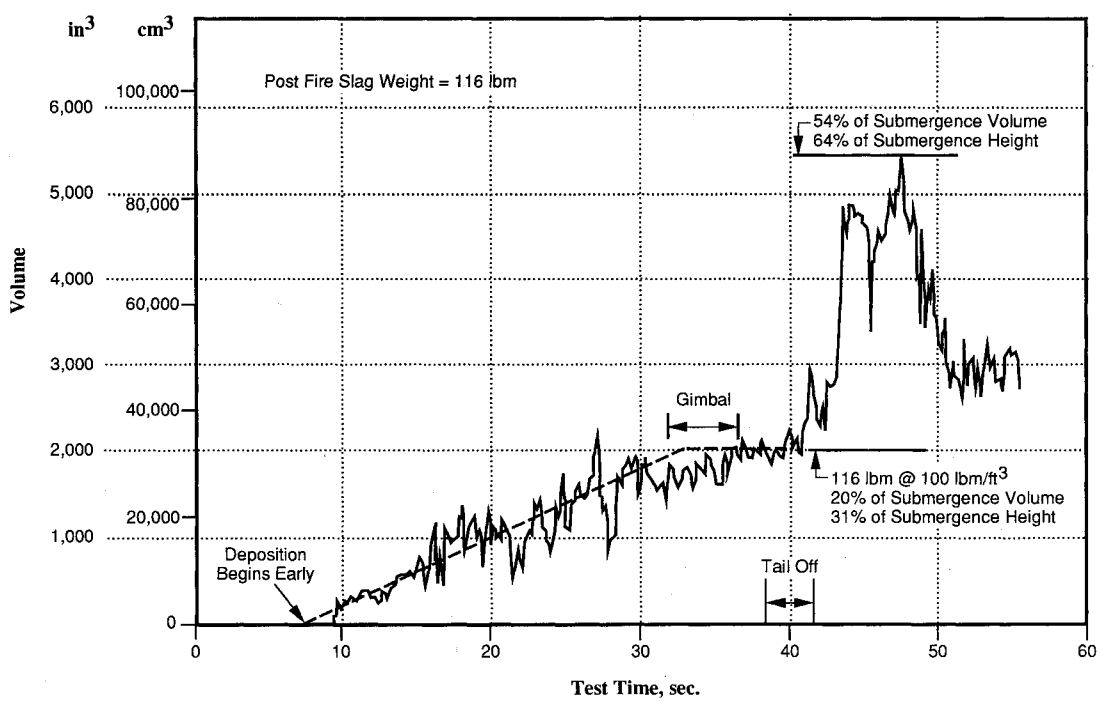

Fig. 7 History of SICBM slag pool volume deduced from RTR of vertically fired motor DS-8.

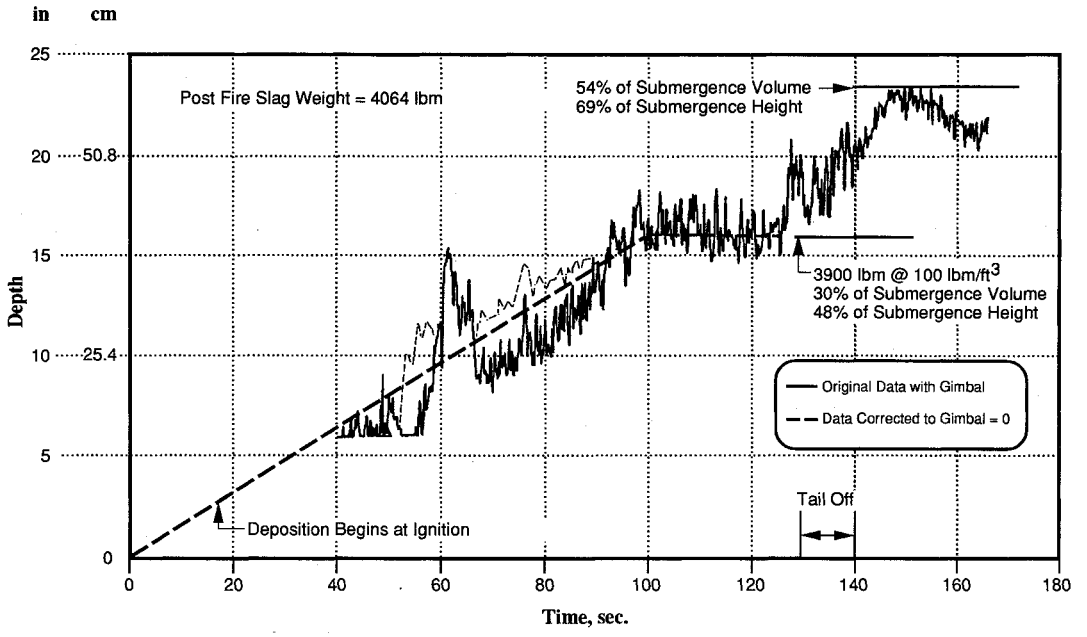

Fig. 8 History of SRMU slag pool depth deduced from RTR of vertically fired motor QM-2.

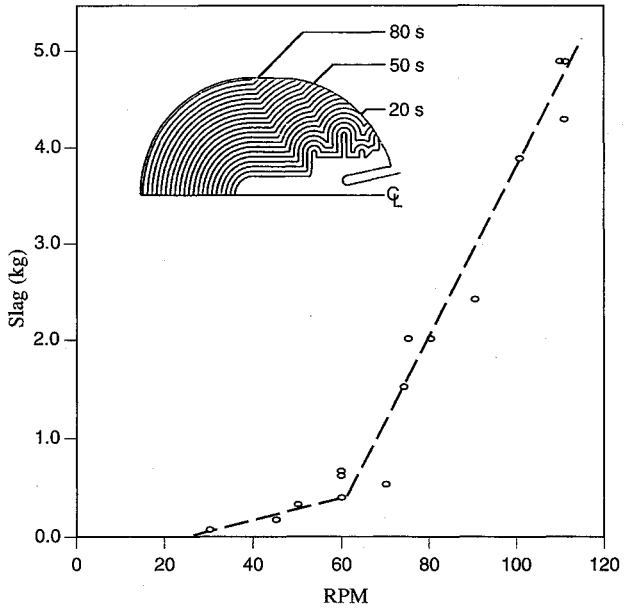

Fig. 9 Effect of spin rate on measured slag weights in statically fired STAR-48 motors.

No reliable slag weights in flight motors have been identified. Slag weights in unrecovered motors have been deduced by correlating trajectory data to predicted vehicle performance, but the uncertainties in the predictions of performance make the deduced slag weights questionable. The only flight motors that have been recovered have been Shuttle Boosters, and slag weights were measured only on seven of the earlier motors; measurements reveal slag weights about one-third that in static motors, but these low weights have been attributed by Boraas[19] to slag ejection during descent and splashdown.

Droplet Size Distributions

The most comprehensive experimental study of droplet size distributions generated by combustion of aluminized solid propellants was conducted[1,2] in the Thiokol Quench Particle Combustion Bomb (QPCB), and included the AP-composite Shuttle Booster and cross-linked double-base SICBM propellants. In each of the 132 tests, a small disk of propellant was burned in a nitrogen atmosphere and the ejected oxide droplets quenched when they plunged into a layer of nonreacting liquid at distances between 2.5 and 15 cm from the propellant surface. Detailed measurements of the resulting size distribution of these quenched particles were then made over the range 0.1 to 600 μm using a sieve stack and Microtrac light-scattering device. Propellants were burned over a wide range of pressures, and the distribution of quenched droplet diameters was always found to be bimodal log-normal; typical results are shown in Fig. 10. Mathematical analysis showed that 70–80% of the particulate mass was contained in "smoke" particles less than 5 μ in diameter whose mass-median diameter was around 1.5 μm at all pressures and for all propellants tested, whereas the remaining 20–30% of the particulate mass had mass-median diameters varying from 40 to 200 μm, depending on pressure and propellant. The standard deviations of the smoke and large-droplet mode were always around $\sigma = 0.4$ and 0.2, respectively. Consequently, since a log-normal distribution of $f(D)$ is defined by

$$f(D) = 0.5[1 + \text{erf}(Z/\sqrt{2})] \quad (1)$$

where $Z = (1/\sigma)\log_{10}(D/D_m)$ and erf is the error function, then if the large-droplet mode has a mass-median diameter $D_m = 50$ μm (for example), then 1) half of the large-droplet mass is smaller than 50 μm (i.e., the definition of mass-median diameter), 2) 93.4% of the large-droplet mass is smaller than 100 μm, and 3) only 1% of the large-droplet mass is larger than 146 μm. Similarly, 91% of the smoke mass is smaller than 5.0 μm, and the Sauter mean diameter of the smoke is $D_{32} = D_m e^{-2.65\sigma^2} = 1.0$ μm.

Despite the implications of Hutchison's correlation, no effect of AP vendor or lot on droplet size has been observed for the RSRM propellant. The original droplet size measurements[1,2] used propellant composed of AP primarily from PE lot 69, also used in static motors DM-8 and DM-9, which generated 2300 lb of slag (Table 1). However, some propellant samples using AP lot 51 were also burned and generated droplet sizes with no significant difference from those using lot 69; unfortunately, no static motor was fired using AP from lot 51, and so no corresponding slag weight is available. More recently, QPCB measurements have been repeated at Thiokol using a new Microtrac device to analyze the entire size range of particulate generated by propellant samples comprised of

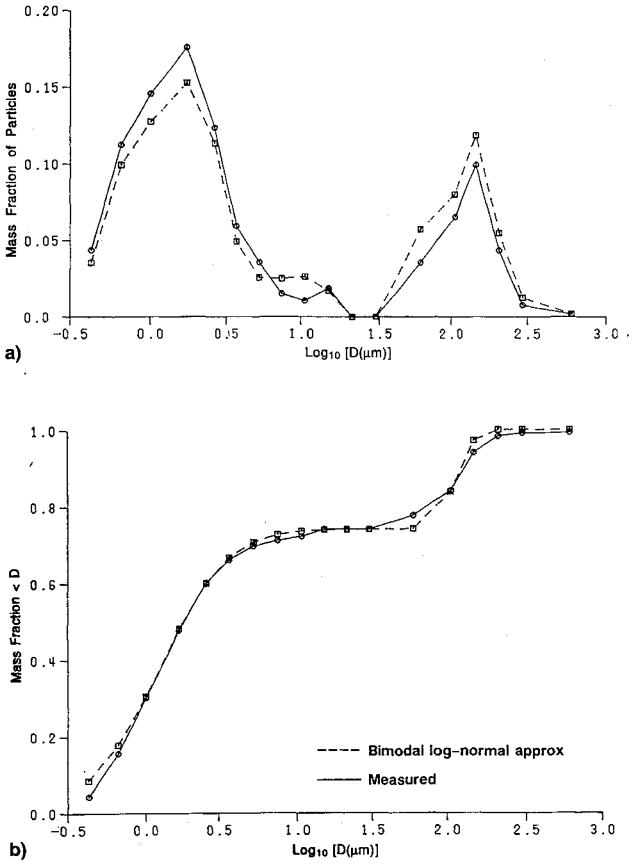

Fig. 10 Typical droplet size distribution obtained from a quench bomb test of Shuttle Booster propellant TP-H1148 at 500 psi: a) bimodal mass distribution in repeat tests and b) bimodal log-normal mass accumulation function.

AP from WECCO, KM, and PE: the PE results were similar to the original data[2] and no significant affect of vendor was evident, although the WECCO generated a slightly larger fraction of smoke.

The intrusiveness of the measurements in the quench bomb and the nonsimilitude of its flowfield compared to full-scale motors has prompted attempts to validate its results both analytically and experimentally. Analytically, intrusiveness and nonsimilitudes have been estimated[2] to affect the measured diameters by less than ±20%, and subsequent use of the nominal quench bomb data in many two-phase flow analyses for a wide range of full-scale motors[2,14,15,20] has resulted in roughly correct predictions of slag weight, droplet/wall impingement, and droplet diameters in plumes. Experimentally, the $D_{32} = 1.0$ μm of the smoke was found to agree identically with the value deduced by Parry and Brewster,[21] using nonintrusive light-scattering in the combustion flame of an AP-composite propellant. Attempts at validating the size distribution of the large-droplet mode have been made by burning samples of Shuttle Booster propellant in the micromotors at the Naval Postgraduate School[22] and analyzing the droplets using nonintrusive laser diagnostics; good agreement was obtained for size measurements made near the propellant surface, but by the time the large droplets reached the nozzle entrance they appeared to have suffered breakup that would not be expected in full-scale motors.

However, support for the mass-median diameters of the large-droplet mode measured in the quench bomb is provided by studies of combustion of single aluminum agglomerates. When aluminized propellants burn, their aluminum powder melts at the surface to form agglomerates of mass-median diameter D_{ag}; curve fits of measured agglomerate data are available in the Solid Propellant Performance Program (SPP)[23]:

Table 6 Values of β deduced from quench bomb data and D_{ag} correlations

Propellant	Pressure, psi	D_m, μm	β
SICBM	500	80	0.52
	1000	55	0.53
	1500	50	0.62
Star-48	500	130	0.68
	1000	101	0.65
Shuttle Booster	50	162	0.50
	200	117	0.58
	500	106	0.74
	1000	90	0.80

for AP-composite propellants, D_{ag} (μm) $= 34.21/f_s^2 r$, where f_s is the solids fraction in the propellant, and r is the burn rate in in./s at the specified pressure. These agglomerates are then blown off the propellant surface by the gaseous products, and burn as they traverse the combustion chamber. The burning occurs in a diffusion flame around the agglomerate, where the vaporizing aluminum meets the oxidizing gas. The aluminum oxide that forms in the flame either diffuses outward to form smoke, or inward to form an ever-enlarging oxide cap at one end of the agglomerate. Thus, the size of an agglomerate changes as the result of several effects: mass loss due to aluminum vaporization, mass gain due to conversion of aluminum to its oxide, and density increase as aluminum converts to its oxide. When the aluminum agglomerate has completely oxidized to smoke and cap, the final mass-median diameter D_m of the cap is a fraction β of the initial agglomerate diameter D_{ag}:

$$D_m = \beta D_{ag} \tag{2}$$

Analytical[24] and experimental[25] studies of burning aluminum droplets have found that the combustion factor β lies between 0.6–0.8, depending in part on pressure; the values of β deduced from quench bomb data (Table 6) lie between 0.50–0.80, and are thus quite consistent with these fundamental results, thereby providing additional confidence in their accuracy. Assuming that the values of β deduced from the Shuttle Booster propellant are applicable to other AP-composite propellants, then the mass-median diameters for Titan IV should be about 100 μm at 1000 psi, and for Castor IV should be about 90 μm at 500 psi.

It must be emphasized that the droplet diameters in the motor chamber are an order of magnitude larger than those in the nozzle and plume because the droplets shatter as they pass through the nozzle.[20,26,27] Consequently, Hermsen's correlation[28] of nozzle and plume droplet sizes are inappropriate for slag calculations.

Some analysts have argued that measured droplet sizes are too large to yield predicted slag weights in agreement with measured values. This is a result of any or all of the following deficiencies in their models: 1) assignment of large-droplet sizes to the entire droplet mass flux, 2) overprediction of slag generation using potential flow analysis or conservative capture rules, and/or 3) excessively high choices for the bulk density of Al_2O_3 as discussed in the next section. In addition, predicted slag weights are required to be greater than measured if significant ejection is occurring.

Droplet Bulk Density

The correct choice of droplet bulk density is critical since studies[14] have shown that slag weight is nearly proportional to droplet density. Droplet bulk density varies strongly with temperature, but the entire body of high-temperature data[29–31] known to this author for aluminum oxide ranges only from 2327–2823 K (Fig. 11). The extrapolation of this data to a typical motor temperature of 3500 K is obviously risky. How-

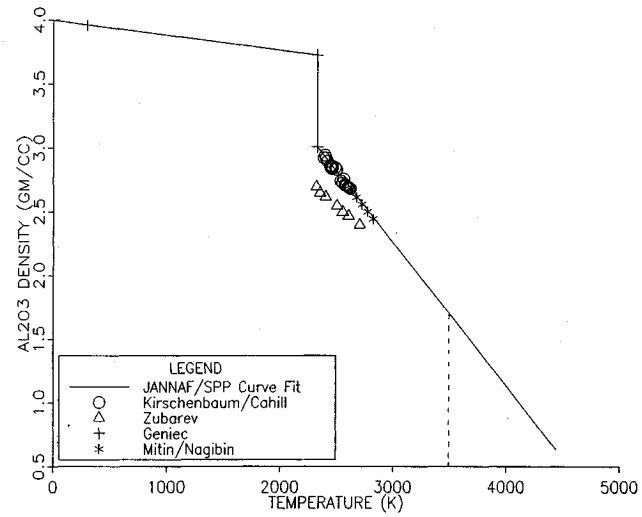

Fig. 11 Available high-temperature data for bulk density of aluminum oxide.

ever, in the absence of any better information, the linear extrapolation recommended by JANNAF seems reasonable:

$$\rho_d \text{ (gm/cc)} = 5.632 - 0.001127 T_d \text{ (K)} \quad (3a)$$

$$\rho_d \text{ (lbm/ft}^3\text{)} = 351.1 - 0.039 T_d \text{ (°R)} \quad (3b)$$

where T_d is usually assumed equal to the adiabatic flame temperature in the chamber. Indeed, densities deduced from measured slag weight and slag-pool volume estimated from 1) RTR films of a burning SICBM motor and 2) slag-pool markings on the wall of the Titan IV (Fig. 2) support this extrapolation, so that a value of 1.6 gm/cc (100 lbm/ft^3) appears to be reasonable at typical motor temperatures.

Droplet Capture Rules

The definitions of the conditions under which droplets are unable to exit the nozzle are herein called the "capture rules." Few modelers recognize the crucial impact of capture rules and that they are the biggest unknowns in slag generation. Two are discussed here: 1) streaming of aluminum agglomerates off the propellant and onto the case wall, and 2) droplet impingement on the backface of the nozzle.

Some modelers[6-10,12-14] have assumed that slag is a result only of two-phase flow, whereby some of the droplets flowing with the gas are unable to turn fast enough to exit through the nozzle; on the other hand, Meyer[11] believes that in spinning motors all gas-borne droplets exit the nozzle and slag is due only to droplets streaming along the wall. The truth probably lies somewhere in between. It is probable that both streaming and gas/droplet flow contribute to slag generation in spinning motors, especially under axial acceleration; it is also possible that streaming of droplets off the grain and along the wall is even a factor in booster motors due to the crossflow along the grain surface, although it is unlikely at late burn times when the bore Mach number becomes small. Wall streaming over significant periods of motor burn would probably introduce large amounts of unburned aluminum into a slag pool behind the nozzle because streams have little surface area for oxidation; indeed, larger than expected quantities of unburned aluminum were deduced during tailoff of SICBM because flashing of the slag pool corresponded better to the vapor pressure of aluminum than that of aluminum oxide. Wall streaming into recirculation zones behind baffles in burning tactical motors[32] is also evident in RTR films.

The key capture rule that is rarely even addressed by modelers is whether the slag generated by two-phase flow is due solely to entrapment of droplets in the recirculation zone, or is also caused by droplet impingement on the backside of the nozzle (Fig. 1). If droplets that strike the nozzle outside the recirculation zone bounce, they will be swept downstream and out the nozzle. However, if they shatter and stick, the resulting layer of droplets may stream along the nozzle surface. The direction of this streaming depends on the relative strength of the shearing action of the gas as opposed to that of vehicle or gravitational acceleration and the surface tension of the layer: if the gas shear dominates, the slag layer will stream out the nozzle, but if acceleration dominates, the slag layer will stream aftward into the slag pool in vertically fired nozzle-down motors, or azimuthally into the slag pool in horizontally fired motors. In the CFD slag studies[14] of SICBM it was found that much too little slag was predicted solely from entrapment, and measured slag weights could be matched only by adding all impinging droplet flow; however, this was probably a consequence of the small recirculation zone in SICBM, as simulated in Fig. 1. It is conceivable that in some situations gas shear might dominate acceleration and reduce slag through ejection. This could explain the low slag weights in static firings of Castor IVB, and the threshhold noted by Eber[18] that a minimum level of axial acceleration is needed before slag accumulation can begin in spinning space motors. Anomalous thrust pulses observed in RSRM and SICBM flight motors might be caused by temporary reversal of the direction of the streaming of impinging droplets out the nozzle instead of into the recirculation zone.

Deficiencies of Potential Flow Models

Many modelers[6-10] have assumed that the gas flowfield is adequately approximated as potential (inviscid, irrotational). However, this is erroneous since viscous and rotational effects have strong impact on slag generation.

Viscous Effects

Viscosity causes the formation in boosters of an extensive recirculation zone behind submerged nozzles after the propellant there has burned away.[3-5] The relative size of the recirculation zones in space motors are smaller because of the radial direction of the flow there.

Since inviscid analysis will not predict the presence of this zone, the location of the separation streamline must be guessed and replaced with a solid boundary. The wrong choice of boundary can have a significant effect on the predicted slag weight; e.g., a potential flow analysis[14] of the SICBM yielded differences of about 25% in predicted slag for two different choices of recirculation zones (I that filled half, vs II that filled most of the SICBM submergence cavity shown in Fig. 12a). However, no affect was identified for different recirculation zones as long as they nearly filled or extended up-

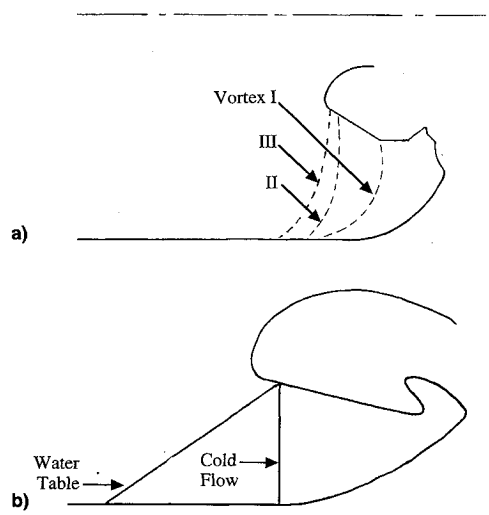

Fig. 12 Choices of separation streamlines used in Thiokol slag studies utilizing potential flow code FLOWNET: a) SICBM long motor[14] and b) Space Shuttle Booster.[33]

stream of the submergence cavity (SICBM separation lines II and III in Fig. 12a, and two choices for the Shuttle Booster[33] shown in Fig. 12b). Alternately, these results may imply that the separation point of flow along the case wall has much less effect on slag weight than does the flow reattachment point on the nozzle backface. It is concluded that viscous modeling is required to minimize these uncertainties.

Rotational Effects

Irrotational flow requires that the gas be ejected from the propellant grain in a nonperpendicular direction, which is physically unrealistic; thus, perpendicular injection yields rotational flow. This is easily seen from the closed-form solutions[34] for incompressible inviscid flow in a semi-infinite cylinder with uniform injection along the sidewall $y = 1$ (Fig. 13a); for irrotational flow

$$u = 2x \qquad v = -y \tag{4}$$

while for rotational flow

$$u = \pi x \cos Z \qquad v = -\sin Z/y \qquad Z = \pi y^2/2 \tag{5}$$

where u and v are, respectively, the axial (x direction) and radial (y direction) components of velocity normalized by the uniform injection velocity, and x and y are normalized by the radius of the cylinder. Thus, the angle of injection in rotational flow is $\tan^{-1}(v/u) = 90$ deg everywhere, as required by the surface boundary condition, but in irrotational flow it decreases rapidly from 90 deg at the head-end to only 5.7 deg five cylinder-radii downstream (Fig. 13a). The validity of rotational Eq. (5) in describing real (i.e., even viscous) flow in a cylindrical combustion port has been demonstrated experimentally by Dunlap et al.[35,36] whereas the inadequacy of irrotational modeling has been discussed by Murdock.[37]

The resulting trajectories of 50-μm droplets are shown in Fig. 13b; it is seen that the incorrect injection required by irrotational flow results in droplet streamlines further from the motor axis and are, therefore, more susceptible to capture in the recirculation zone. This explains why the droplets of Fendell et al.[8] are ejected nonperpendicularly from the cylindrical and aft faces of the propellant grain and will greatly overpredict the slag generation rate.

Irrotational flow may not be unreasonable for late burn times when no propellant remains in the aft-end of the motor (as long as an appropriate recirculation zone is imposed), so that the gas and droplet flow is predominantly axial, or in space motors where the predominantly radial flow generates small recirculation zones (Fig. 14). This may explain why the slag weight predicted for PAM-63F by Debolt et al.[10] agrees fairly well with the measured value.

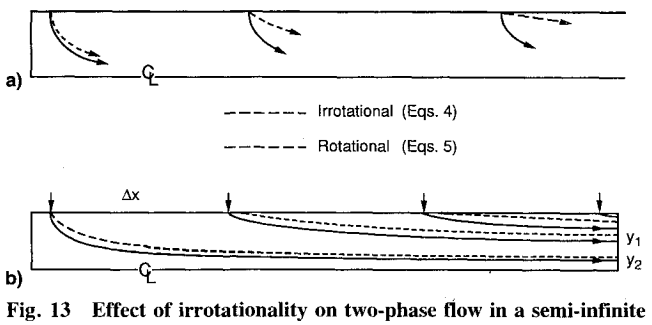

Fig. 13 Effect of irrotationality on two-phase flow in a semi-infinite cylindrical duct: a) typical gas streamlines showing nonperpendicular injection in irrotational flow and b) streamlines of 50-μm droplets showing outward bias in irrotational flow.

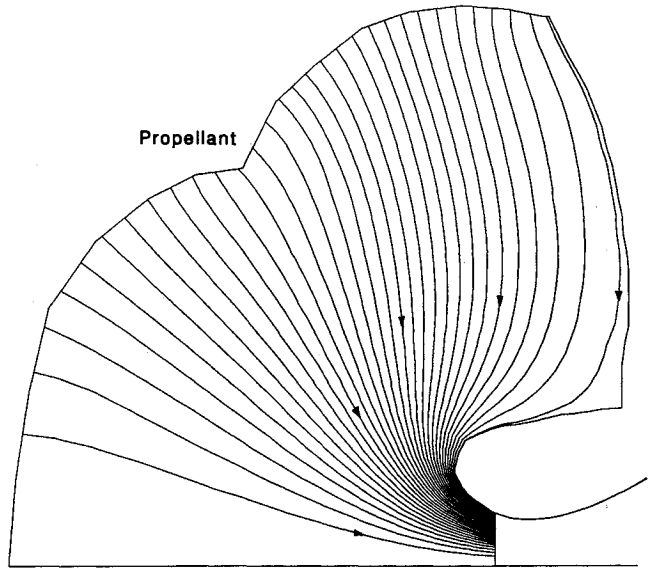

Fig. 14 VORSTREM simulation of gas streamlines in PAM-63D at 40-s burn time (note negligible recirculation zone).

Deficiencies of Recent Slag Modeling

Having summarized what is known about slag generation, it is now possible to expose the deficiencies of previous modeling efforts. Common deficiencies exhibited by these previous models are summarized in Table 7.

The earliest slag modeling was carried out by Boraas[6] for the Space Shuttle Booster, but was hampered by a lack of 1) an appropriate viscous flow code for submerged nozzles, and 2) droplet size and density data. He assumed compressible potential gas flow (inviscid, irrotational) to drive a monomodal distribution of droplet sizes scaled from incomplete data for a different propellant. The extent of the recirculation region behind the submerged nozzle was approximated from momentum considerations with the results corrected using cold-flow data. He described for the first time many of the key issues in slag generation, and astutely concluded that the variation in slag weights from static firings of the Shuttle Booster might be caused by only slight variations in the propellant composition of the two center segments. However, his overprediction of droplet bulk density [3.0 gm/cc (185 lbm/ft^3)] and neglect of droplet size bimodality resulted in the erroneous deduction that slag accumulation began only late in the motor burn; had he chosen a correct density and bimodal size distribution he would have deduced slag accumulation to begin near midburn.[38]

Haloulakis[7] applied the Boraas technique in an attempt to explain slag generation in spinning space motors; however, no value of droplet bulk density nor rationale for his separation streamline was reported, and erroneous (plume rather than chamber) droplet data was used that was an order of magnitude too small. Although Eq. (2) and quench bomb data for the STAR propellant at typical motor pressures yields a large-droplet mass-median diameter of about 90 μm, Haloulakis found that he needed a mass-median diameter only around 10 μm to match measured STAR slag weights; even if he had (erroneously) combined the modes into an effective monomodal distribution, the mass-median diameter should have been about 20 μm. This requirement for undersized droplets was probably a result of using Boraas' high droplet density and of bookkeeping all impinging droplets as captured when many probably stream out the nozzle. He also referred to "solid" particles, even though aluminum oxide is liquid at chamber temperature.

Fendell et al.[8] conducted an incompressible slag analysis of the SICBM booster that correctly used available QPCB droplet size data; unfortunately, their results were jeopardized by

Table 7 Common deficiencies in slag modeling

Phase	Characteristic	Deficiency
Gas	Potential flow	Irrotationality yields non-perpendicular gas injection from propellant surface.
		Inviscidness can't identify recirculation zone or wall shear-layer or bump-induced separation.
		Spinning of gas ignored in spinning motors.
	Domain	Aft-end computational domain requires known inlet flow.
	Droplet size	Measured bimodal log-normal distribution replaced erroneously by monomodal or single value.
		Presence of large smoke mass ignored.
		Large effects of subtle propellant variations ignored.
		Plume or nozzle sizes applied to chamber.
	Density	Wrong value chosen; extrapolation dangerous.
	Flowfield	Full gas/droplet coupling ignored.
		Slag generation deduced to begin too late.
		Alteration of flowfield boundary due to slag ignored.
	Capture rule	Either streaming or gas/droplet flow ignored.
		Impinging droplets assumed retained.
		Ejection ignored.

mysterious choices for their recirculation zone and droplet density [only 4.0 gm/cc (245 lbm/ft^3) was cited for room temperature], the inappropriate use of potential flow at early burn times, and overestimation of the amount of aluminum oxide by neglect of the aluminized gaseous species (see the Slag Bookkeeping section below).

Smith-Kent et al.[9] used the same gas/droplet codes as Boraas in an attempt to simulate slag generation in SICBM and Castor IVB; agreement with measured Castor IVB slag weight was attained only by using droplet diameters much smaller than predicted by Eq. (2). Debolt et al.[10] modeled the slag generation in Titan IV SRMU and PAM-63F space motor using an incompressible potential flow analysis without a recirculation region; agreement with measured SRMU slag weight was attained only by using droplet diameters 56% larger than predicted by Eq. (2).

Meyer[11] proposed that slag generation in spinning and axially accelerating space motors is caused not by two-phase flow, but by an acceleration vector that drives droplets along the propellant surface and onto the wall instead of into the flow; although wall streaming is probably important in these motors, Golafshani and Loh[13] have shown that two-phase flow also will contribute to slag accumulation in spinning space motors. Furthermore, it is disconcerting that Haloulakis and Meyer were both able to match slag accumulation in PAM-D spinning space motors assuming two very different mechanisms (two-phase flow vs wall streaming).

Some models[13,14] have solved only the aft-end motor domain in order to save computational time. Consequently, they have been forced to assume the distribution of gas and droplet velocities and droplet flux along the bore inflow boundary. This has introduced large errors into the slag predictions, and masked the effects of upstream slots and inhibitor stubs.

Most models have assumed isothermal gas and droplet fields in the chamber and, therefore, ignored the energy equations; however, it has been shown by Sabnis et al.[39] that distributed combustion of the droplets creates nonuniformities in the gas temperature and droplet mass fraction throughout the chamber.

Modelers have not yet accounted for the nondilute effect of the swirling gas/dense-droplet cloud or for droplet collision/coalescence suggested by the RTR films of the recirculation zone during motor burn. It is clearly not the simple gas flow with dilute droplet phase that has typically been modeled.

Most modelers have not addressed the possibly large effects that subtle changes in boundary shapes can have, e.g., due to the growth of the slag pool or slag layers on the case wall or nozzle backface (Fig. 2). Wall bumps at case joints or changes in insulation thickness may cause premature flow separation at critical locations near the recirculation zone. Propellant coning near the case wall due to accelerated burning (caused by precure diffusive migration of propellant constituents) might change the ejection angle of gas and droplets in just that region where most captured droplets originate.

Most modelers have ignored 1) the effect of crossflow on the droplet ejection boundary condition at the propellant surface, 2) the effect of turbulence on droplet trajectories first exposed by Madabhushi et al.,[40] and 3) the momentum and energy extracted from the gas to accelerate the droplets. Models have typically been validated only for a single motor family (e.g., only boosters or only space motors, but not both).

Most modelers have not addressed the large effects that subtle differences in propellant characteristics can contribute to slag generation as in Fig. 7, which can result in significantly different slag weights in supposedly identical motors (as in Table 1). The variability of the capture rules among motors and during the burn of a single motor has not been addressed, let alone understood.

Improved Gas Flow Modeling

In recent years a number of two-phase compressible viscous CFD codes have been developed for modeling internal flows in rocket motors; some examples are Thiokol's SHARP,[13] SRA's CELMINT,[15] and Aerospace's IS[41] or WW[42] as applied by Misterek et al.[43] to space motors. These codes are uniformly valid at any Mach number and, therefore, can predict the flowfield throughout the chamber and nozzle. They are time-accurate and allow for laminar or turbulent modeling. They are fully coupled to the droplet phase, and CELMINT allows for gaseous chemical reactions and distributed combustion of the droplets.[39] Unfortunately, they are expensive to run and require expert knowlege of CFD in order to generate meaningful results. Consequently, simplified schemes are desirable for day-to-day design and anomaly studies. This has led to the questionable use of potential flow models.

One simplified two-dimensional scheme (VORSTREM) that avoids the pitfalls of the irrotational/inviscid potential-flow model has been developed by Salita,[44] and utilizes the streamfunction/vorticity formulation of the unsteady incompressible Navier-Stokes equations. Incompressibility is far less of a deficiency for slag modeling than is irrotationality, because compressibility becomes important only in the nozzle inlet while irrotationality directly affects droplet trajectories everywhere in the chamber. The normalized equations for Ψ and ω are then of similar and relatively simple form:

$$\Psi_{xx} + \Psi_{yy} = y^e\omega + \varepsilon u \tag{6}$$

$$\omega_{xx} + \omega_{yy} = Re(W + \omega_\tau)/\mu + \varepsilon(\omega/y - \omega_y)/y + S \tag{7}$$

where

$$u = y^{-\varepsilon}\Psi_y, \qquad v = -y^{-\varepsilon}\Psi_x, \qquad \omega = u_y - v_x$$

$$W = (\omega u)_x + (\omega v)_y, \qquad Re = \rho UL/\mu_0$$

and ε is 0 for planar flow or 1 for axisymmetric flow, and S accounts for variable viscosity and momentum exchange with the droplets. Gas streamlines are directly identified as lines of constant Ψ, and the viscous capability allows prediction of a recirculation zone whose extent will vary with Re. Note that the potential flow equation is recovered by setting $\omega = 0$, and that solving Eqs. (6) and (7) is little more difficult than solving two potential flow equations. Boundary conditions and solution methods for these equations are discussed in detail by Roache[45] and Gosman et al.[46] Once the grid and viscosity model have been supplied, only Reynolds number, time step, and the upwind differencing factor for the convective terms W need be specified. Equations (6) and (7) have been solved in laminar flow ($S = 0$) by Salita[44] on body-fitted grids for the PAM-63D at a single burn time (Fig. 14), and for the RSRM, SICBM, and SRMU at multiple burn times. The PAM and RSRM flowfields have been shown to agree well with those predicted by the CFD code SHARP,[13] and the RSRM gas streamlines late in burn are shown in Fig. 15 to agree qualitatively with the water table simulation (Fig. 2). Although this simplified technique has its limitations, reasonable flowfields have been generated at six motor burn times in the course of a single workday.

Improved Droplet Flow Modeling

Two-phase flows are fully coupled in that the gas accelerates the droplets, and expends momentum and energy to do so. In addition, it has been shown using CELMINT[39] that aluminum droplet combustion occurs over a much larger portion of the motor chamber than previously believed, thereby creating temperature variation of about 20% in the gas flowfield and mass exchange with the gas. Thus, the best droplet flow modeling will include the energy equation and be coupled to the gas. The advantages and disadvantages of achieving this coupling by solving the droplet phase using either a Lagrangian (follow each droplet) or Eulerian (follow the cloud) formulation has been discussed elsewhere.

Unfortunately, the solution of the fully-coupled and reacting system of equations is often too expensive for many applications, and the final accuracy of the predictions is limited more by the uncertainties in the capture rules and choices of droplet parameters like size and density. Consequently, since the velocity and thermal lags are relatively small in the chamber, it is common to ignore the effect of the droplets on the gas as a first approximation, resulting in a quasicoupled flowfield.

Droplet trajectories in quasicoupled flowfields are determined by integrating the droplet momentum equations by following an individual droplet (Lagrangian scheme). The droplet data required for the analysis is exposed by the droplet momentum equations:

$$\frac{dw_d}{dt} = G_d(w_g - w_d) + g_w \tag{8}$$

where

$$G_d = (18\mu/\rho_d D^2)(C_D Re_d/24), \quad Re_d = \rho|w_g - w_d|D/\mu \tag{9}$$

and w_g and w_d are, respectively, the gas and droplet velocity components in either the axial or radial direction, and g_w is the imposed acceleration in the direction of w. Thus, once the gas and acceleration fields are specified, the only other parameters that must be defined in order to solve the droplet trajectories are the droplet diameter D, its bulk density ρ_d, and its C_D. Once the trajectories are known, capture rules must be chosen to determine slag deposition rate.

Table 8 Sets of five discrete diameters for $\sigma = 0.2$ to simulate slag generation

	Uniform subfractions			Large-droplet emphasis		
n	Δf_n	f_n	D_n/D_m	Δf_n	f_n	D_n/D_m
1	0.20	0.10	0.554	0.30	0.15	0.620
2	0.20	0.30	0.785	0.30	0.45	0.944
3	0.20	0.50	1.000	0.20	0.70	1.273
4	0.20	0.65	1.273	0.10	0.85	1.612
5	0.20	0.75	1.805	0.10	0.95	2.135

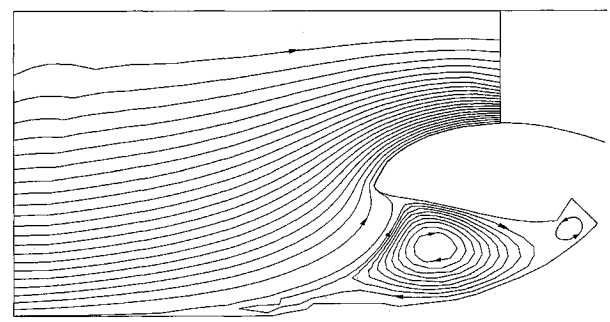

Fig. 15 VORSTREM simulation of gas streamlines in RSRM late in the burn (note the agreement with the water table results) (Fig. 2).

If the droplet size distribution has not been measured, estimates can be made using Eqs. (1) and (2), with $\beta = 0.65$ and $\sigma = 0.2$. Bulk density should be determined from Eq. (3). The choice of a droplet drag law is simplified in the combustion chamber by the fact that the gas flow regime is continuum, and the velocity and thermal lags are small enough that droplet distortion from spherical is minimal. Since most drag laws in the continuum regime apply to spherical droplets and are nearly the same, the effect of drag law on droplet trajectories in the chamber is relatively unimportant. The effect of acceleration up to 10 g on droplet trajectories has been shown[12,14] to be negligible in boosters because the droplet inertia in the aft-end of the motor is high.

For slag modeling, the continuous distribution of diameters (as in Fig. 10) must be simulated by an adequate set of N discrete sizes. Only the large-droplet mode needs simulation because most of the smoke is small enough to turn into the nozzle and exit the motor. Salita[2] demonstrated that the large-droplet size distribution must be simulated by at least three, but preferably more discrete diameters or predicted slag weight would be much too low in RSRM.

The N discrete diameters D_n are identified by subdividing the continuous distribution of droplet mass into N subfractions Δf_n, and choosing D_n to lie at the midmass value f_n of each fraction. For a log-normal mass distribution defined by Eq. (1), f_n determines Z_n, so that $D_n/D_m = 10^{\sigma Z_n}$. The subfractions are sometimes chosen as uniform, but it is probably better for slag calculations to emphasize the larger droplets; as an example, the discrete sizes for five groups are compared in Table 8. Trajectories of 245-μm droplets in the RSRM at 80-s burn time are shown in Fig. 16, using the gas field shown in Fig. 15.

Proper Slag Bookkeeping

Once the droplet trajectories have been predicted, an estimate of slag deposition rate can be made. This estimate will depend on the fraction of Al_2O_3 in the flow, and especially on the chosen capture rule.

The mass fraction of propellant that burns to aluminum oxide is $F_0 = (B\phi - C)(1 - U) + U\phi$, where B is the stoichiometric ratio 1.8895 for burning aluminum to alumi-

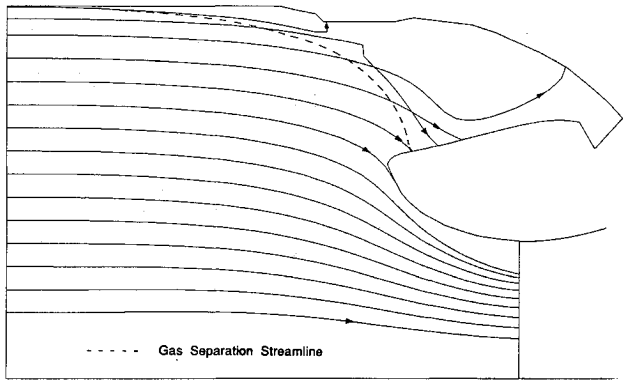

Fig. 16 Predicted trajectories of 245-μm droplets through flowfield of Fig. 15.

num oxide, C is the mass fraction of aluminum that burns to gaseous species like $AlCl_x$ and Al_xO_y, and U is the fraction of aluminum in the propellant that does not burn. Most booster and space motors utilize propellants with aluminum loadings ϕ between 0.16–0.20, and are large enough that combustion is essentially complete, so that $U \approx 0$. Any standard thermochemistry code will determine C as well as the adiabatic flame temperature.

Wherever the computational domain extends to the propellant surface, then the droplet flux entering the domain is F_0. However, for aft-end computational domains (Figs. 15 and 16) the inflow boundary cuts across the bore where the flux of larger droplets is nonuniform due to upstream velocity lags; consequently, an estimate must be made of this nonuniformity. For example, for the semi-infinite cylindrical bore shown in Fig. 13, the mass flux of droplets of a given size must be constant between trajectories that leave the grain surface an axial distance Δx apart, and arrive at axial location x at radial locations y_1 and y_2; if the gas flowfield is approximated by Eqs. (5), then the distribution of droplet flux at location x and $y = (y_1 + y_2)/2$ will be

$$F_n(x, y) = F_0/[F_0 + (1 - F_0)\delta]$$

where

$$\delta = (\sin Z_{n2} - \sin Z_{n1})x/\Delta x \qquad (10)$$

Trajectory studies like that shown in Fig. 13 have confirmed that for small droplets $\delta = 1$ and $F_n = F_0$ everywhere. However, larger droplets will concentrate closer to the motor centerline; typical flux distributions are shown in Fig. 17 for RSRM.

The suggested procedure for calculating slag deposition rate is as follows:

1) A capture rule is defined, in particular a critical radial location y_c along the surface of the submerged nozzle, outboard of which impinging droplets will be retained in the motor. Typical choices are the nosetip or the reattachment point of the separation streamline that encloses the recirculation zone; however, it may be some other location that actually oscillates in time and differs among motors.

2) One of the discrete droplet sizes is chosen from Table 8, and a droplet is placed either at a point on the propellant surface if it lies within the computational domain, or at a specified radius on the inflow boundary.

3) The droplet is allowed to flow downstream; if it exits the nozzle or impinges inboard of y_c, another droplet of the same diameter is placed at a larger radius on the inflow boundary.

4) Steps 2 and 3 are repeated until a critical radius r_c is found such that droplets originating there barely impinge on the nozzle at the critical radius y_c. Thus, all droplets of this

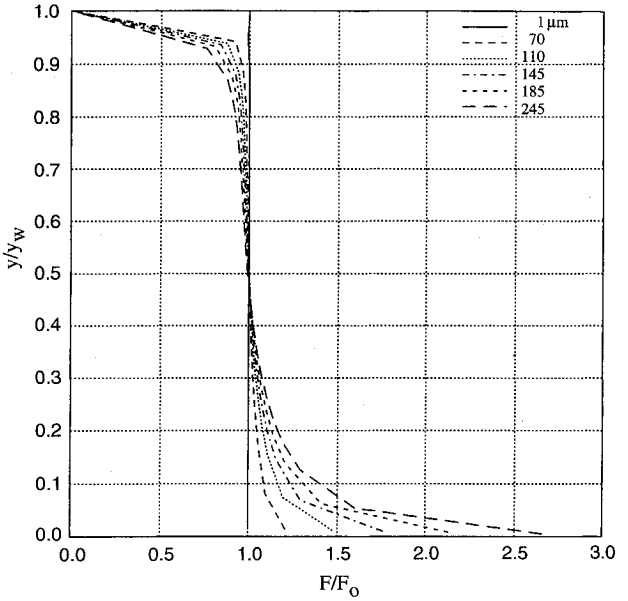

Fig. 17 Predicted distribution of droplet flux exiting a cylindrical bore with gas flowfield defined by Eq. (5).

size originating outside of r_c are defined to be retained as slag. (The trace of r_c with burn time is equivalent to Fendell's separatrix.[8])

5) The total gas + droplet flow rate m_d outside r_c is determined by integration. The resulting mass flow rate of the chosen nth droplet size will then be $F_n\alpha(m_d)_n\Delta f_n$, where F_n is the effective mass fraction of droplet size n outside r_c, α is the fraction of the oxide contained in the large mode, and Δf_n is the mass fraction of the large-droplet mode discretized as D_n.

6) Steps 2–5 are repeated for all discrete droplet diameters D_n, and the total slag deposition rate at this time is calculated from the sum $\alpha \Sigma F_n(m_d)_n\Delta f_n$.

7) Steps 1–6 are carried out for at least four motor burn times, and the resulting deposition rate is integrated in time to identify the total deposition weight for that capture rule.

The appropriate choice of capture rule is not yet understood. Matching the measured slag weight in the long SICBM motor required retention of all impinging droplets outboard of the nosetip, because the recirculation zone was small and deep in the submergence cavity.[14] On the other hand, recent modeling by Salita of slag generation in the RSRM[47] and SRMU indicates that 1) roughly 40% of the impinging droplet mass strikes the nozzle very close to the nosetip, and is thus susceptible to ejection; and 2) this impingement mass must be ejected in order to match the measured slag weights.

Although flight acceleration up to 10 g had a negligible effect on droplet trajectories in boosters, it may have a significant effect on the capture rules by preventing droplets from streaming around the nozzle nosetip.

Conclusions

Slag generation in solid rocket motors is a very complex phenomenon, as evidenced by the many questions raised by full-scale motor data. Previous efforts to simplify its simulation have been inadequate, so it is time to review what is known and not known about slag generation. It is concluded that

1) Potential flow analysis cannot predict the recirculation zone that dominates slag generation, and requires a physically-erroneous nonperpendicular injection of both gas and droplets from the propellant grain. Consequently, flow modeling should only be conducted using viscous rotational methods; results of a simple incompressible stream function/vor-

Table 9 Steps to a reliable prediction of slag

Step	Function	Reference
1	Measure droplet size distribution from nominal propellant	1, 2
2	Account for variability in propellant (vendors, grinds, etc.)	49, 50
3	Account for changes in droplet size due to motor spin, axial acceleration, and incomplete combustion	——
4	Extrapolate bulk density of Al_2O_3 to chamber temperature	29–31
5	Develop turbulence model for two-phase internal flow	40
6	Develop reliable CFD gas flowfield model	13, 15, 39–42, 44
7	Develop reliable droplet tracking routine	14
8	Account for droplet streaming along case wall if important	11
9	Determine capture rules for slag retention along nozzle backface	Fig. 1
10	Account for droplet interactions in submergence cavity	48
11	Account for possible grain coning at wall	——
12	Account for effect of wall bumps on gas flow separation	Fig. 15
13	Account for three-dimensional effects of aft-end fins and vector duty cycle	——
14	Account for flight acceleration on droplet trajectories/capture	14
15	Adjust measured slag for possible ejection, washout, junk	——

ticity model have been shown to predict flowfields in agreement with more general CFD models.

2) Many previous studies of slag generation have used erroneous droplet-size distributions, thereby leading to erroneous conclusions about the duration of slag generation and the validity of their flow analysis. Quench bomb measurements for a wide range of propellants suggest that droplet-size distributions are bimodal log-normal, with small ("smoke") droplets of mass-median diameter of roughly 1.5 μm, comprising 70–80% of the droplet mass, and the large-droplet mode of mass-median diameters ranging from 50–200 μm, comprising only 20–30% of the mass. No inconsistencies have been found between these quench bomb results and a wide range of other measurements and analyses, despite the intrusiveness and nonsimilitude of its environment compared with that in full-scale motors.

3) Predicted slag weights are nearly proportional to the value of bulk density of aluminum oxide. Many previous models of slag generation have chosen densities that were much too high. Although the correct value at chamber temperature must be extrapolated from lower-temperature data, a value of 1.6 gm/cc (100 lbm/ft^3) seems to be reasonable.

4) The process of droplet capture and retention as slag is not well understood. For a motor like SICBM with a small recirculation zone deep in the submergence cavity, direct entrainment contributes only a small fraction of measured slag weight, so that a large fraction of the impingement layer must be retained. However, in motors with large recirculation zones like RSRM (Figs. 2 and 15), direct entrainment provides slag weight in agreement with measurement, so that most of the nozzle slag layer must be ejected. The variable behavior of this nozzle-wall slag layer may indeed explain many surprising slag generation results, such as the absence of slag in Castor IVB. The nozzle-wall layer may flow into the recirculation zone if acceleration is high enough, or out the nozzle if gas shear and wall shape allow; oscillatory behavior such as periodic buildup and sluffing of this layer might explain the pressure pulses attributed to slag ejection. Streaming of aluminum agglomerates along the case wall might also contribute to slag in booster motors, as postulated for spinning space motors.

5) Although gravity and vehicle acceleration up to 10 g have been shown to have little affect on droplet trajectories in boosters, they may have a significant affect on the capture rules. Thus, motors with little slag in static firings might generate large slag in flight if acceleration reverses the direction of the flow of the nozzle-wall slag layer.

6) Subtle changes in propellant characteristics like AP-vendor and lot number appear to have a large affect on slag generation, but not due to their effect on Al_2O_3 droplet size.

Recommendations

1) Greater care is required in future slag modeling to ensure that the results are meaningful; the recommended steps to a more reliable prediction of slag accumulation are summarized in Table 9.

2) The two-phase flow in the Castor IVB should be modeled to determine the attribute of its design that resulted in negligible slag in spite of high slag potential.

3) Tests of burning propellant in a windowed slab motor with submerged nozzle should be conducted 1) to determine if crossflow causes streaming of aluminum agglomerates along the propellant surface and onto the case wall, 2) to identify those parameters affecting the direction of flow of the slag layer on the back-face of the nozzle, and 3) to provide experimental data against which comparisons of CFD predictions of the recirculation zone can be made.

Acknowledgments

Although the positions stated in this article are those of the author, the data leading to these positions would not have been available without the important contributions of many Thiokol researchers. These include the quench bomb testing of Paul Braithwaite, Wendell Christensen, Fox Daugherty, and Paul Roberts; the CFD modeling of Mehdi Golafshani and Roy Loh; the fundamental studies of Stan Boraas; and the tabulation and analysis of slag data by Boyd Hutchison, Kyle Speas, and Fred Perkins. Helpful discussions about slag ejection were held with Charlie Martin of NASA MSFC.

References

[1]Braithwaite, P. C., Christensen, W. N., and Daugherty, V., "Quench Bomb Investigation of Aluminum Oxide Formation from Solid Rocket Propellants (Part I): Experimental Methodology," *Proceedings of the 25th JANNAF Combustion Meeting*, Vol. 1, 1988, pp. 178–184 (CPIA 498).

[2]Salita, M., "Quench Bomb Investigation of Al_2O_3 Formation from Solid Rocket Propellants (Part II): Analysis of Data," *Proceedings of the 25th JANNAF Combustion Meeting*, Vol. 1, 1988, pp. 185–197 (CPIA 498).

[3]Robbins, S. M., and Boraas, S., "Water Table Studies of SRM Internal Flows," Thiokol Corp. Videos, May 1983.

[4]Waesche, R. H. W., Sargent, W. H., and Marchman, J. F., "Space Shuttle Solid Rocket Motor Aft-End Internal Flows," *Journal of Propulsion and Power*, Vol. 5, No. 6, 1989, pp. 650–656.

[5]"Final Report of the Space Shuttle SRM Cold Flow Tests," Thiokol Rept. TWR-10604, July 1975.

[6]Boraas, S., "Modeling Slag Deposition in the Space Shuttle Solid Rocket Motor," *Journal of Spacecraft and Rockets*, Vol. 21, No. 1, 1984, pp. 47–54.

[7]Haloulakos, V. E., "Slag Mass Accumulation in Spinning Solid

Rocket Motors," *Journal of Propulsion and Power*, Vol. 7, No. 1, 1991, pp. 14–21.

[8]Hess, E., Chen, K., Acosta, P., Brent, D., and Fendell, F., "Effect of Aluminized-Grain Design on Slag Accumulation," *Journal of Spacecraft and Rockets*, Vol. 29, No. 5, 1992, pp. 697–703.

[9]Smith-Kent, R., Perkins, F., and Abel, R., "A Potential Two-Phase Flow Model for Predicting SRM Slag," AIAA Paper 93-2307, June 1993.

[10]Debolt, R., Acosta, P., and Brent, D., "Slag in Aluminized Solid Rocket Motors," Chemical Propulsion Information Agency, 30th JANNAF Propulsion Meeting, Nov. 1993.

[11]Meyer, R. X., "In-Flight Formation of Slag in Spinning Solid Propellant Rocket Motors," *Journal of Propulsion and Power*, Vol. 8, No. 1, 1992, pp. 45–50.

[12]Johnston, W. A., Murdock, J. W., Koshigoe, S., and Than, P. T. "Slag Accumulation in the Titan SRMU," AIAA Paper 94-3279, June 1994.

[13]Golafshani, M., and Loh, H.-T., "Computation of Two-Phase Viscous Flow in Solid Rocket Motors Using a Flux-Split Eulerian-Lagrangian Technique," AIAA Paper 89-2785, July 1989.

[14]Salita, M., Smith-Kent, R., Golafshani, M., Loh, H.-T., Abel, R., and Pratt, D., "Prediction of Slag Accumulation in SICBM Static and Flight Motors," Thiokol TWR-40259, Sept. 12, 1990.

[15]Sabnis, J. S., De Jong, F. J., and Gibeling, H. J., "Calculation of Particle Trajectories in Solid Rocket Motors with Arbitrary Acceleration," *Journal of Propulsion and Power*, Vol. 8, No. 5, 1992, pp. 961–967.

[16]Blomshield, F. S., Kraeutle, K. J., and Stalnaker, R. A., "Shuttle Redesigned Solid Rocket Motor Aluminum Oxide Investigations," 31st JANNAF Combustion Meeting, Oct. 1994.

[17]Frederick, R. A., "DS-8 Slag Accumulation Analysis," Sverdrup/AEDC Memo 90-294, Sept. 1990.

[18]Eber, R. M., "Slag Retention Predictions in Large Solid Propellant Rocket Motors," AIAA Paper 91-2294, June 1991.

[19]Boraas, S., "SRM/RSRM Slag Motion Study," Thiokol TWR-50405, May 1990.

[20]Salita, M., "Implementation and Validation of the One-Dimensional Gas-Particle Nozzle Flow Code OD3P," *Proceedings of the 26th JANNAF Combustion Meeting*, Vol. II, 1989, pp. 69–82 (CPIA 529).

[21]Parry, D. L., and Brewster, M. Q., "Optical Constants of Al_2O_3 Smoke in Propellant Flames," *Journal of Thermophysics and Heat Transfer*, Vol. 5, No. 2, 1991, pp. 142–149.

[22]Laredo, D., McCrorie, J. D., Vaugh, J. K., and Netzer, D. W., "Motor and Plume Particle Size Measurements in Solid Propellant Micromotors," *Journal of Propulsion and Power*, Vol. 10, No. 3, 1994, pp. 410–418.

[23]Nickerson, G. R., et al., "The Solid Propellant Rocket Motor Performance Prediction Computer Program (SPP), Version 6.0, Vol. I," AFAL-TR-87-076, Dec. 1987.

[24]Bhatia, R., and Sirignano, W. A., "Metal Particle Combustion with Oxide Condensation," *Combustion Science and Technology* (submitted for publication).

[25]Turns, S. R., Wong, S. C., amd Ryba, E., "Combustion of Aluminum-Based Slurry Agglomerates," *Combustion Science and Technology*, Vol. 54, 1987, pp. 299–318.

[26]Pilch, M., and Erdman, C. A., "Use of Breakup Time Data and Velocity History Data to Predict the Maximum Size of Stable Fragments for Acceleration-Induced Breakup of a Liquid Droplet," *International Journal of Multiphase Flow*, Vol. 13, No. 6, 1987, pp. 741–757.

[27]Craig, J. E., "Conventional and Liquid Metal Droplet Breakup in Aerodynamic Nozzle Contractions," AIAA Paper 84-0201, Jan. 1984.

[28]Hermsen, R. W., "Aluminum Oxide Particle Size for Solid Rocket Motor Performance Prediction," *Journal of Spacecraft and Rockets*, Vol. 18, No. 6, 1981, pp. 483–490.

[29]Kirschenbaum, A. D., and Cahill, J. A., "The Density of Liquid Aluminum Oxide," *Journal of Inorganic Nuclear Chemistry*, Vol. 14, 1960, pp. 283–287.

[30]Mitin, B. S., and Nagibin, Yu. A., "Density of Molten Aluminum Oxide," *Zhurnal Fizicheskoi (Russian Journal of Physical Chemistry)*, Vol. 44, No. 5, pp. 1325, 1326, 1970; also *Chemical Abstracts*, 48707v.

[31]Zubarev, U. V., "Certain Properties of Molten (Liquid) Aluminum Oxide" (translated by M. I. Weinreich), *Inorganic Materials Series* (USSR Academy of Sciences), Vol. 5, No. 9, pp. 1563–1565, 1969.

[32]Davis, D. K., "Slag Formation in Solid Propellant Rocket Motors," *Proceedings of the 24th JANNAF Propulsion Meeting*, Vol. I, 1987, pp. 35–46 (CPIA 480).

[33]Carpenter, N. M., "Effect of Separation Region Geometry on Maximum Escaping Particle Size," Thiokol Rept. TWR-17881, Jan. 3, 1988.

[34]Culick, F. E. C., "Rotational Axisymmetric Mean Flow and Damping of Acoustic Waves in a Solid Propellant Rocket," *AIAA Journal*, Vol. 4, No. 8, 1966, pp. 1462–1464.

[35]Dunlap, R., Willoughby, P. G., and Hermsen, R. W., "Flowfield in the Combustion Chamber of a Solid Propellant Rocket Motor," *AIAA Journal*, Vol. 12, No. 10, 1974, pp. 1440–1442.

[36]Dunlap, R., Blackner, A. M., Waugh, R. C., Brown, R. S., and Willoughby, P. G., "Internal Flowfield Studies in a Simulated Cylindrical Port Rocket Chamber," *Journal of Propulsion and Power*, Vol. 6, No. 6, 1990, pp. 690–704.

[37]Murdock, J. W., "Comment on 'Simple Modeling of Particle Trajectories in Solid Rocket Motors,'" *Journal of Propulsion and Power*, Vol. 10, No. 3, 1994, pp. 437, 438.

[38]Boraas, S., private communication, April 1993.

[39]Sabnis, J., De Jong, F., and Gibeling, H., "A Two-Phase Restricted Equilibrium Model for Combustion of Metalized Solid Propellants," AIAA Paper 92-3509, July 1992.

[40]Madabhushi, R. K., Sabnis, J. S., De Jong, F. J., and Gibeling, H. J., "Calculation of the Two-Phase Aft-Dome Flowfield in Solid Rocket Motors," *Journal of Propulsion and Power*, Vol. 7, No. 2, 1991, pp. 178–184.

[41]Chang, I.-S., "An Efficient Intelligent Solution for Viscous Flows Inside Solid Rocket Motors," AIAA Paper 91-2429, July 1991.

[42]Wang, J. C. T., and Widhopf, G. F., "An Efficient Finite-Volume TVD Scheme for Steady-State Solutions of the 3D Compressible Euler/Navier-Stokes Equations," AIAA Paper 90-1523, June 1990.

[43]Misterek, D. L., Murdock, J. W., and Koshigoe, S., "Gas-Dynamic Flow in a Spinning, Coning Solid Rocket Motor," *Journal of Propulsion and Power*, Vol. 9, No. 1, 1993, pp. 35–42.

[44]Salita, M., "VORSTREM: A Simple and Versatile 2D Viscous Solver for Chamber Flow in Solid Rocket Motors," AIAA Paper 94-2779, June 1994.

[45]Roache, P. J., *Computational Fluid Dynamics*, Hermosa, Albuquerque, NM, 1976.

[46]Gosman, A. D., Pun, W. M., Runchal, A. K., Spaulding, D. B., and Wolfshtein, M., *Heat and Mass Transfer in Recirculating Flows*, Academic Press, 1969.

[47]Salita, M., "Prediction of RSRM Slag Generation Using VORSTREM/TD2P," TRW IOM F757.MS.94-001, Jan. 1994.

[48]Salita, M., "Use of Water and Mercury Droplets to Simulate Al_2O_3 Collision/Coalescence in Rocket Motors," *Journal of Propulsion and Power*, Vol. 7, No. 4, 1991, pp. 505–512.

[49]Hutchison, B., "Ammonium Perchlorate Slag Correlation," Morton Thiokol Memo L211-FY89-M074, March 1989.

[50]Marin, L., "Slag Generation in Spinning Bates Motors," *Proceedings of the 27th JANNAF Propulsion Meeting*, Vol. IV, 1990, pp. 259–293 (CPIA 315).